Chromosoma (2006) 115: 15–26
DOI 10.1007/s00412-005-0037-1

MINI-REVIEW

Roderick Y. H. Lim · Ueli Aebi · Daniel Stoffler

From the trap to the basket: getting to the bottom of the nuclear pore complex

Received: 12 October 2005 / Revised: 12 November 2005 / Accepted: 21 November 2005 / Published online: 10 January 2006

Abstract Nuclear pore complexes (NPCs) are large supramolecular assemblies that perforate the double-membraned nuclear envelope and serve as the sole gateways of molecular exchange between the cytoplasm and the nucleus in interphase cells. Combining novel specimen preparation regimes with innovative use of high-resolution scanning electron microscopy, Hans Ris produced in the late eighties stereo images of the NPC with unparalleled clarity and structural detail, thereby setting new standards in the field. Since that time, efforts undertaken to resolve the molecular structure and architecture, and the numerous interactions that occur between NPC proteins (nucleoporins), soluble transport receptors, and the small GTPase Ran, have led to a deeper understanding of the functional role of NPCs in nucleocytoplasmic transport. In spite of these breakthroughs, getting to the bottom of the actual cargo translocation mechanism through the NPC remains elusive and controversial. Here, we review recent insights into NPC function by correlating structural findings with biochemical data. By introducing new experimental and computational results, we reexamine how NPCs can discriminate between receptor-mediated and passive cargo to promote vectorial translocation in a highly regulated manner. Moreover, we comment on the importance and potential benefits of identifying and experimenting with individual key components implicated in the translocation mechanism. We conclude by dwelling on questions that we feel are pertinent to a more rational understanding of the physical aspects governing NPC mechanics. Last but not least, we substantiate these uncertainties by boldly suggesting a new direction in NPC research as a means to verify such novel concepts, for example, a de novo designed 'minimalist' NPC.

This article is dedicated to the memory of Hans Ris.

Communicated by E.A. Nigg

R. Y. H. Lim · U. Aebi (✉) · D. Stoffler
M.E. Müller Institute for Structural Biology,
Biozentrum, University of Basel,
4056 Basel, Switzerland
e-mail: Ueli.Aebi@unibas.ch
Tel.: +41-61-2672261
Fax: +41-61-2672109

Introduction

It was in November 1989, during the 29th Annual Meeting of the American Society for Cell Biology in Houston, that Hans Ris presented a poster with absolutely startling stereo electron micrographs of nuclear envelopes (NEs) isolated from newt and frog oocytes (Ris 1989). More specifically, as documented by Fig. 1a, these electron micrographs revealed the cytoplasmic and nuclear peripheries of the NPC surface topography with a hitherto unparalleled clarity and detail. This was achieved by manually dissecting an isolated oocyte nucleus into low salt buffer, from where it was transferred onto a glass coverslip, extracted with Triton X-100, opened with fine glass needles, fixed, dehydrated with ethanol, critical point dried, and ion-beam sputtered with a thin layer of Pt. The sample was then imaged by high-resolution field emission in-lens scanning electron microscopy (FEISEM) at low voltage. Accordingly, the cytoplasmic face of the NE (Fig. 1a, lower right) is closely packed with NPCs exhibiting an 'annulus' with eight 'cylindrical particles' protruding and a 'central particle' residing in most pores. In contrast, the nuclear face of the NE (Fig. 1a, upper half) unveils distinct 'fishtraps,' which sit atop the NPCs. For the first time, these pictures documented a pronounced asymmetry of the cytoplasmic and NPC periphery.

To prepare cross-sections of NEs for low voltage FEISEM imaging, Ris and his coworkers cut corresponding 200- to 300-nm-thick Epon sections of chemically fixed or cryo-immobilized oocyte nuclei and extracted the plastic with an epoxy removal crown ether complex. After washing, the sections were mounted on a carbon layer, dehydrated with ethanol, and critical point dried. Metal coating of these preparations was generally not required for low voltage FEISEM. Figure 1b reveals a stereo pair of a prepared and imaged oocyte NE cross-section. A side view

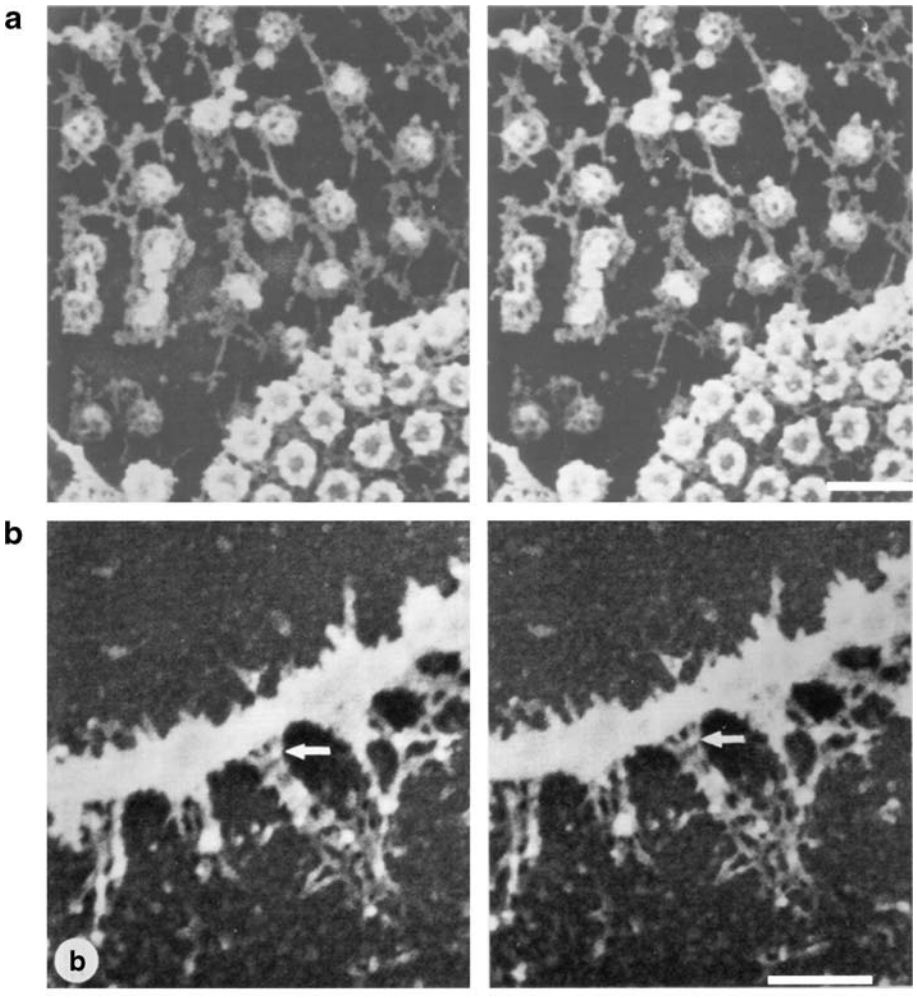

Fig. 1 Stereo electron micrographs of nuclear envelopes (NEs) isolated from **a** newt and **b** frog oocytes. **a** The cytoplasmic surface of the NE is depicted at the *lower right*, closely packed with NPCs consisting of a pronounced annulus 'decorated' with eight 'cylindrical particles'. A 'central particle' is depicted in most NPCs as well. In the *upper half*, we look down onto the intranuclear surface of the NE. Accordingly, distinct 'fishtraps' representing the intranuclear peripheral segments, i.e., the 'nuclear baskets' of the NPCs between the fishtraps, are scattered remnants of the nuclear lamina fibers, disrupted, during swelling of the NEs in low salt buffer. **b** Cross-section (~250 nm thick) through an isolated NE from a *Xenopus laevis* oocyte. A side view of a fishtrap (marked by an *arrow*) is depicted, with the tip of the arrow pointing to a small ring at the top of the fishtrap. A cable-like structure is attached to the ring projecting radially into the nucleus. Scale bars in **a** and **b**, 200 nm. Reprinted from Ris and Malecki, J Struct Biol 111:148–157 (1993) with permission from Elsevier

of a fishtrap (more commonly known nowadays as the nuclear basket) is depicted by the white arrow, with the tip of the arrow pointing to a distinct 50-nm ring at the top of the fishtrap, from where a cable-like assembly projects into the nuclear space. Evidently, these novel nuclear supramolecular assemblies form part of a branched, hollow cable system connecting NPCs with the nuclear interior (Ris and Malecki 1993). These stereo images, which represent some of the most spectacular and informative electron micrographs found in literature to this day, have started a new chapter in the history of NPC structure. In fact, these remarkable ultrastructural data have challenged many researchers in the field—including ourselves—to replicate, scrutinize, and elaborate on these novel views of NPC architecture (Aebi et al. 1990; Akey 1990; Jarnik and Aebi 1991; Goldberg et al. 1997; Kiseleva et al. 1998; Stoffler et al. 2003; Beck et al. 2004). Last but not least, Ris' morphological data also had a profound impact on the molecular dissection of NPC structure (Pante and Aebi 1993; Pante et al. 1994; Fahrenkrog et al. 1998; Rout et al. 2000; Fahrenkrog et al. 2002; Paulillo et al. 2005).

Imaging the nuclear pore complex

It has been demonstrated that NPCs can undergo massive structural changes induced by cellular signals such as calcium or nucleotides (Jarnik and Aebi 1991; Stoffler et al. 1999b, 2003; Fahrenkrog and Aebi 2003), suggesting that the NPC as a whole is extremely sensitive to environmental conditions and can exhibit significant structural plasticity, which in turn may be crucial for efficient cargo translocation through its central pore. Hence, a mechanistic understanding of nucleocytoplasmic transport at the level of the response of individual NPCs requires that these distinct functional states be visualized, characterized, and identified.

During the past decade, NPCs have been imaged with a variety of imaging modalities. Because a given method either provides only partial insight or is subject to preparative and/or experimental artifacts due to the size and complexity of the specimen under investigation, structure determination is best achieved with a hybrid approach where experimental data are gathered by different

data acquisition methods and under a variety of preparation conditions. Figure 2 depicts NPCs imaged by various microscopy techniques. Accordingly, side views of NPCs can best be obtained from cross-sections of embedded NPCs, depicting cytoplasmic filaments and nuclear baskets (Fig. 2a). With this method, the height of the nuclear baskets was determined to be ~120 nm for *Xenopus* NPCs and ~100 nm for yeast NPCs (Fahrenkrog et al. 1998). This method is also useful for mapping nucleoporins within the 3-D architecture of the NPC using antinucleoporin antibodies in combination with colloidal-gold particles (cf. Pante et al. 1994; Fahrenkrog et al. 1998, 2002; Rout et al. 2000). Cryo-electron microscopy (EM) images of NPCs embedded in a thick layer of amorphous ice clearly depict the eightfold rotational symmetry of the NPC (Fig. 2b), and the distal ring of the nuclear basket centered above the central channel of the NPC (Fig. 2b, inset). Metal-shadowing after quick-freeze/freeze-drying (or critical point drying) for EM allows for an improved 3-D impression of the NPC (Fig. 2c,d), particularly when using stereo images. Atomic force microscopy, also known as scanning force microscopy (SFM), allows for the direct visualization of the surface topography of one and the same specimen in its physiological buffer environment in various stages of activity, thus enabling to directly correlate structural and functional responses of biological matter at a submolecular resolution (Stolz et al. 2000). Figure 2e,f depicts the cytoplasmic and the nuclear faces, respectively, of native NPCs kept 'alive' in near-physiological buffer (Stoffler et al. 1999b). As the highly flexible cytoplasmic filaments and the filamentous architecture of the fragile nuclear baskets cannot be resolved by SFM, the cytoplasmic face of the NPC appears doughnut-like (Fig. 2e), whereas its nuclear face exhibits a dome-like morphology (Fig. 2f). More specifically, the cytoplasmic face of the native NPCs yields doughnut-like rings protruding by ~35 nm from the NE surface (Fig. 2e) revealing indications of the eightfold rotational symmetry of individual NPCs. In contrast, the nuclear baskets (Fig. 2f) of the native NPCs appear as ~75-nm high dome-like structures, which are susceptible to mechanical damage, by the scanning tip.

3-D reconstructions of the nuclear pore complex: a brief history

The 3-D architecture of the NPC has been unveiled by extensive EM studies including 3-D reconstructions of amphibian NEs, according to which the vertebrate NPC exhibits a tripartite architecture with an eightfold rotational symmetry, a maximum diameter of ~120 nm in the plane of the NE, an overall dimension of ~180 nm perpendicular to the plane of the NE, and a total mass of ~125 MDa (Reichelt et al. 1990; Jarnik and Aebi 1991; Hinshaw et al. 1992; Akey and Radermacher 1993; Goldberg et al. 1997;

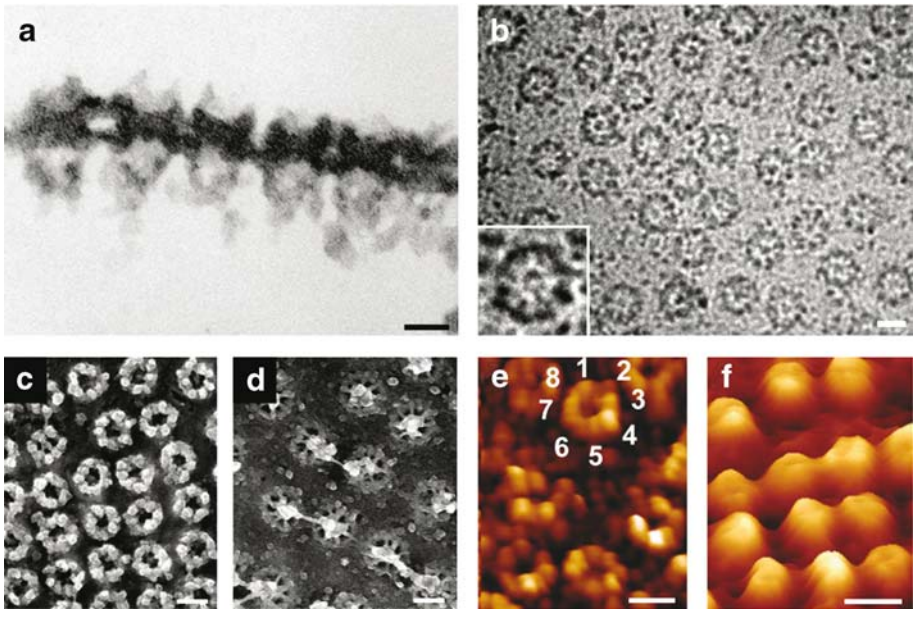

Fig. 2 Imaging the nuclear pore complex (NPC) by various microscopy techniques. **a** Thin-section of embedded nuclear envelope (NE) imaged by transmission electron microscopy (TEM). The cytoplasmic filaments and the nuclear basket are readily visible. **b** Energy-filtered electron microscopy (EFTEM) image of NE embedded in thick (200–300 nm) amorphous ice. The inset clearly depicts the eightfold rotational symmetry of the NPC and the distal ring of the nuclear basket centered above the central channel of the NPC. Metal-shadowed, quick-frozen/frozen-dehydrated TEM images of the **c** cytoplasmic and **d** the nuclear face of the NE. This imaging technique allows for a more 3-D impression of the individual NPCs. Individual nuclear baskets on the nuclear face are easily discriminated. **e**, **f** Corresponding scanning force microscopy (SFM) images of the NE kept 'alive' in a near-physiological buffer environment reveal a distinct morphology for **e** the cytoplasmic and **f** the nuclear face. Scale bars in panels **a**–**f**, 100 nm **a**–**f**, 100 nm. **a**, **c** and **d** reproduced with permission from *Nature Reviews* Molecular Cell Biology 4:757–766 copyright (2003) Macmillan Magazines Ltd. **b** reprinted from Stoffler et al. J Mol Biol 328:119–130 (2003) with permission from Elsevier. **e** and **f** reprinted from Stoffler et al. Curr Opin Cell Biol 11:391–401 (1999) with permission from Elsevier

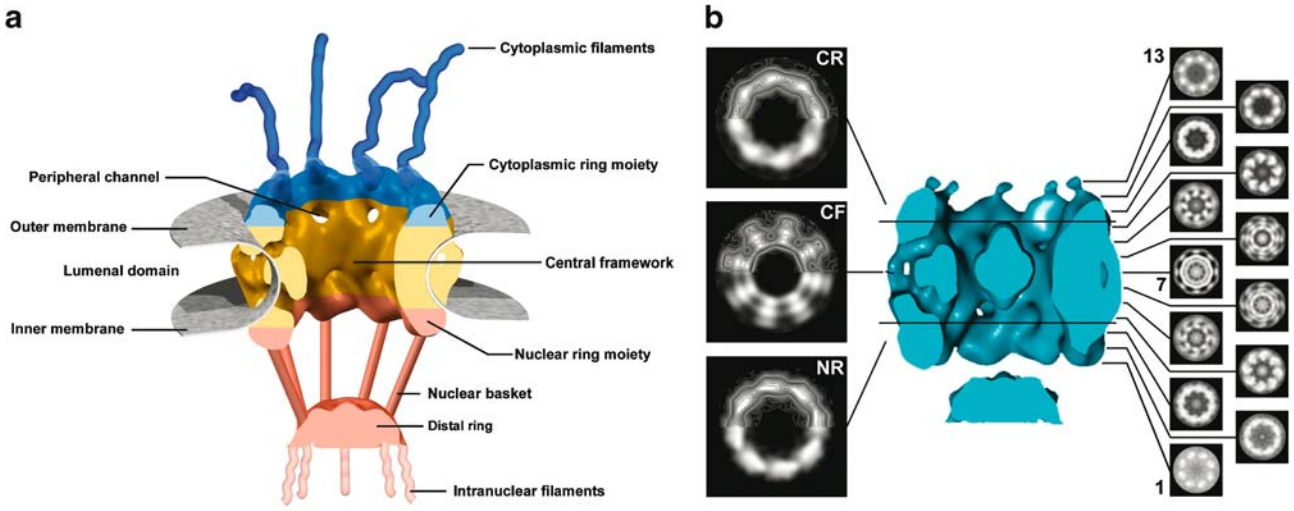

Fig. 3 **a** Current consensus model of the three-dimensional architecture of the nuclear pore complex. The main structural components include the central framework (*yellow*), the cytoplasmic ring moiety (*blue*) and attached cytoplasmic filaments (*blue*), and the nuclear ring moiety (*orange*) and the distal ring (*orange*) of the nuclear basket. The cytoplasmic filaments and the struts of the nuclear basket were modeled into the architecture with software developed at The Scripps Research Institute (Sanner et al. 2005), based on thin-section images of embedded NPCs. **b** Cross-sections through the central framework calculated from the 3-D map (*middle panel*). *Left panel*: the central framework (*CF*) is averaged over slices 4–10, its cytoplasmic ring moiety (*CR*) over slices 11–13 and its nuclear ring moiety (*NR*) over slices 1–3. *Right panel*: cross-sections through 3-D reconstruction in 6-nm steps. See text for details. **a** reproduced with permission from *Nature Reviews* Molecular Cell Biology 4:757–766 copyright (2003) Macmillan Magazines Ltd. **b** reprinted from Stoffler et al. J Mol Biol 328:119–130 (2003) with permission from Elsevier

Stoffler et al. 1999a, 2003; Fahrenkrog and Aebi 2002; Beck et al. 2004).

As depicted in Fig. 3a, the ~55-MDa central framework of the NPC, i.e., the NPC moiety residing in the double-membrane of the NE, consists of eight spokes, sandwiched between a ~32 MDa cytoplasmic ring moiety and a ~21 MDa nuclear ring moiety (Reichelt et al. 1990). From the cytoplasmic ring, eight ~50-nm long, kinky filaments emanate, whereas the nuclear ring is capped with a cage-like structure termed 'fishtrap' (Ris 1989) or nuclear 'basket', which is assembled from eight tenuous, ~75-nm long filaments joined distally by a massive 30- to 60-nm diameter distal ring. The ring-like central framework harbors a large central pore, which serves as the main gateway in signal-dependent, receptor-mediated bidirectional nucleocytoplasmic transport. The central pore often appears plugged with a 'particle' of variable size and appearance, termed central 'plug' or 'transporter' (Akey 1990; Reichelt et al. 1990; Jarnik and Aebi 1991; Akey and Radermacher 1993; Kiseleva et al. 1998). The functional role of the plug remains to be established, although it is possible for this polymorphic structure to consist of a combination of dynamically interacting phenylalanine–glycine (FG)-domains and cargo being caught in transit, rather than representing a stationary component of the NPC (Jarnik and Aebi 1991; Stoffler et al. 1999b, 2003).

The 3-D reconstruction of detergent-released (*dform*), negatively stained *Xenopus* NPCs further revealed that the central framework of the NPC exhibits a high degree of 822 symmetry, i.e., eightfold symmetric relative to its central axis, and twofold symmetric relative to its central plane (Hinshaw et al. 1992). The 822 symmetrized 3-D map exhibits eight distinct peripheral channels with an average diameter of ~9 nm, which were suggested to represent sites for passive diffusion of ions and small molecules (Hinshaw et al. 1992). A 3-D reconstruction of *dform Xenopus* NPCs imaged in amorphous ice (Akey and Radermacher 1993) unveiled similar basic features for the domain architecture of the central framework. It further yielded a massive, hollow transporter being seated in the central pore and exhibiting a tripartite morphology. The transporter was believed to span the width of the central channel. Due to its high variability among distinct NPCs, this central transporter/plug was omitted in the Hinshaw et al. (1992) reconstruction. Similar to the 3-D reconstruction in negative stain, eight peripheral channels could be mapped, although the radial position of these putative diffusion channels was distinct from that of Hinshaw et al. (1992).

Compared to the *dform* NPCs, the 3-D reconstruction of membrane-associated (*mform*) *Xenopus* NPCs in amorphous ice revealed significant differences in the relative location, orientation, and interactions of the radial spokes comprising the central framework (Akey and Radermacher 1993). Contrary to the *dform* NPCs, the central plug was omitted in the 3-D reconstruction of these *mform* NPCs. The observed structural differences between the *dform* and *mform* 3-D reconstructions might have been caused by detergent extraction (*dform*), osmotic shock within the lumen of the NE, and/or mechanical distortions during specimen preparation. Mechanical distortions and surface tension might also have led to a collapse of the cytoplasmic filaments and the nuclear baskets during specimen preparation so that these peripheral structural components were not visible in the *dform* and *mform* 3-D maps.

It is noteworthy that the overall 3-D architecture of the NPC appears to be conserved from yeast to higher

eukaryotes, although the linear dimensions might vary among different species (Fahrenkrog et al. 1998; Yang et al. 1998; Cohen et al. 2002; Stoffler et al. 2003). Accordingly, a 3-D map of the yeast *dform* NPC from frozen-hydrated specimens (Yang et al. 1998) provided a direct comparison with the vertebrate *dform* NPC (Akey and Radermacher 1993). The 3-D reconstruction of the yeast NPC revealed a rather flat ~822 symmetric NPC without, however, exhibiting a distinct cytoplasmic or nuclear ring moiety. Similar to the vertebrate *dform*, the yeast 3-D reconstruction revealed eight peripheral channels within the central framework. Consistent with its smaller linear dimensions, the mass of the yeast NPC was determined to be ~60 MDa (Rout and Blobel 1993; Yang et al. 1998). The yeast NPC is therefore significantly more compact than the vertebrate NPC when the overall dimensions of the yeast and vertebrate 3-D reconstructions are compared, because based on its volume its mass would amount to only ~30 MDa. The existence of cytoplasmic filaments and a nuclear basket has also been documented for the yeast NPC (Fahrenkrog et al. 1998), which again, could not be depicted in the 3-D reconstruction (Yang et al. 1998).

The current consensus model of the nuclear pore complex

The most recent vertebrate NPC 3-D reconstruction was achieved by employing energy-filtering transmission electron microscopy (EFTEM) and tomographic 3-D reconstruction of fully native (i.e., no detergent treatment, no chemical fixation, and no heavy metal staining) *Xenopus* oocyte NEs embedded in thick (i.e., 200–300 nm) amorphous ice (Stoffler et al. 2003). The novel structural insights thereby gained were incorporated into a reformed model (Fig. 3a) that makes a first attempt to also include possible mechanistic aspects of nucleocytoplasmic transport at the single nuclear pore level. As documented in Fig. 3b, the 3-D map of the averaged NPC exhibits a strong eightfold rotational symmetry of the central framework with a rather tenuous plug residing in the central pore. The central framework is perforated by eight peripheral holes (Fig. 3a,b) with a ~10 nm diameter. Radially attached to the central framework are eight distinct ‘handles’ that might actually reside in the lumen of the double-membraned NE, thereby anchoring the NPC within the NE.

Located above the nuclear entry of the central pore is a distinct massive ring-like structure (Fig. 3a,b), evidently representing the distal ring of the NPC's nuclear basket. The distal ring revealed eight ‘bumps’, most likely representing the attachment sites of the struts forming the nuclear basket. In support of this, previous experiments with critical point dried amphibian NEs investigated by FEISEM revealed hollow cables of 50 nm in diameter consisting of eight 6-nm thick filaments that emanated from the distal rings of the nuclear baskets and reached deeply into the nucleus (Ris and Malecki 1993; Ris 1997). Similarly, NPC-attached, p270/Tpr-containing intranuclear filaments forming bundles, which projected as much as 350 nm into the nuclear interior, were identified after *Xenopus* oocytes were chemically fixed and centrifuged (Cordes et al. 1997). The molecular composition and functional significance of these hollow cables or intranuclear bundles, however, remain to be established. It is interesting that this latest vertebrate tomographic 3-D reconstruction indicates that eight ‘stumps’ emanate from the distal ring toward the nuclear interior (Fig. 3a), most likely being the anchoring sites of the intranuclear filaments. In fact, the intranuclear filaments were cut off right above the distal ring during the reconstruction process (Stoffler et al. 2003).

On the cytoplasmic face, rudiments of the eight cytoplasmic filaments decorating the cytoplasmic ring moiety were resolved (Fig. 3b). Due to the high flexibility of the cytoplasmic filaments, it was not possible to capture them in a unique spatial conformation, so that only their anchoring sites could be enhanced (Stoffler et al. 2003).

Although not enforced in the tomographic 3-D reconstruction, the central framework of the NPC appears to consist of two similar halves that have been assembled back-to-back (Fig. 3b, left and middle panel). After closer inspection the nuclear ring moiety of the central framework looks slightly more massive compared to the cytoplasmic ring moiety (Fig. 3b). Cross-sections through the central framework in 6-nm steps confirmed this impression (Fig. 3b, right panel). Slice 1 cuts the nuclear ring moiety close to its nuclear surface, whereas slice 12 yields a cross-section of the cytoplasmic ring moiety close to its cytoplasmic surface. Slice 7 represents the midplane of the central framework. The 13 cross-sections also depict the pronounced vorticity of the central framework. The nuclear half (Fig. 3b, slices 1–6) exhibits an anticlockwise vorticity, which turns via slice 7, as it has no net vorticity, into a clockwise vorticity of the cytoplasmic half (Fig. 3b, slices 8–13), just as described by Akey and Radermacher (1993) for their *dform* NPC.

More recently, these structural features were confirmed and elaborated further by investigating transport-active, intact nuclei from *Dictyostelium discoideum* by means of cryoelectron tomography (Beck et al. 2004). The most variable structural moiety of the NPC is a rather tenuous central plug (discussed below), partially obstructing the central pore and being mobile. Its mobile character was previously documented by SFM (Stoffler et al. 1999b, 2003; Bustamante et al. 2000).

Nuclear pore complex dynamics revealed by scanning force microscopy

As outlined above, understanding the structural details implicated in signal-dependent, receptor-mediated transport of cargos in and out of the nucleus through the NPC has started to unfold, mostly by means of electron microscopy. However, given the limitations of the technique, it is unlikely that this method will be the tool of choice to dissect the more dynamic features of macro or supramolecular machines and to directly correlate struc-

tural with functional states in situ. Scanning force microscopy, on the other hand, has evolved to the point where it is now possible to record surface topographies of native biological material in its physiological buffer environment at near-molecular detail and to directly correlate structural changes with distinct functional states (reviewed in Stolz et al. 2000).

During the past several years, many laboratories have succeeded in visualizing NPCs by SFM (Pante and Aebi 1993; Braunstein and Spudich 1994; Goldie et al. 1994; Oberleithner et al. 1994, 1996; Folprecht et al. 1996; Perez-Terzic et al. 1996; Rakowska et al. 1998; Jaggi et al. 2003a,b). However, none of these examinations were conducted on fully native NPCs. In all cases, the material was chemically fixed, exposed to detergents, or dehydrated and rehydrated at some stage during its preparation for SFM. Hence, it remains unclear whether the responses of NPCs to effector molecules depicted in some of these studies did indeed represent bona fide structural changes or distinct functional responses to adding effectors or ligands, or whether they were merely due to specimen preparation effects (for example, differential extraction of labile or weakly bound NPC constituents or deformations caused by surface tension). To overcome these limitations, a new isolation/preparation protocol for *Xenopus* oocyte NEs was required to avoid exposure to detergents, chemical fixation, or dehydration/rehydration steps. Therefore, SFM imaging conditions were established allowing repeated scanning of these native NE samples in a buffered environment so that one and the same NPC could be watched in response to chemical effectors (Stoffler et al. 1999b; Wang and Clapham 1999). Specifically, time-lapse SFM was employed to monitor structural changes occurring at the cytoplasmic or the nuclear periphery of the NPC, upon adding or removing micromolar amounts of calcium to or from the surrounding buffer medium (Stoffler et al. 1999b).

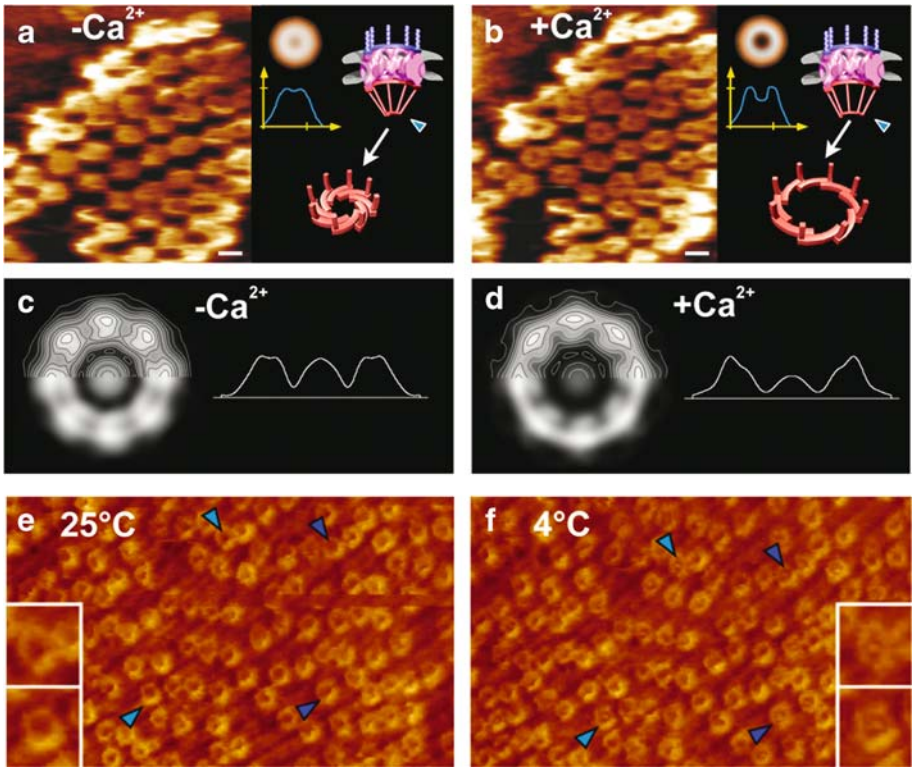

Fig. 4 Imaging native nuclear pore complexes (NPCs) kept functional in near-physiological buffer by scanning force microscopy (SFM). Panels **a** and **b** reveal reversible calcium-mediated structural changes of the nuclear baskets (i.e. the distal rings) by time-lapse SFM of the same individual NPCs. **a** In absence of calcium, the distal rings are 'closed'. **b** Adding 100 μM calcium to the buffer medium opens the distal rings. This process is reversible (for example, by adding 1 mM EGTA which selectively chelates calcium). Calcium only affects the opening of the distal ring of the nuclear basket, not its overall height, as shown in the averaged radial height profiles in **a** and **b**. The 3-D models in **a** and **b** depict the tentative interpretation of the opening and closing of the distal ring upon changing the calcium concentration. In this model, the distal ring might act as an iris-like diaphragm. For better comparison in **c** and **d**, the same individual NPCs were marked with *blue arrowheads*. The effect of calcium on the entire NPC as examined by energy-filtered transmission electron microscopy (EFTEM) of completely unfixed/unstained NEs embedded in thick (200–300 nm) amorphous ice by so-called zero-loss imaging. Single-particle averages, both displayed as grey-level/±contours representations and radial mass density profiles of 100 NPCs each in the **c** absence and **d** presence of calcium reveal significant structural rearrangements within the entire NPC. **e**, **f** Watching temperature-dependent plugging or unplugging of individual NPCs by time-lapse SFM. The same specimen area, adsorbed with its nuclear face, was imaged by SFM in contact mode at **a** 25°C and after cooling the system down to **b** 4°C. In panels **e** and **f**, previously unplugged individual NPCs become plugged upon lowering the temperature. Four corresponding NPCs are marked by *blue arrowheads* for better comparison. *Insets* represent magnifications of two NPCs marked by *blue arrowheads*. All scale bars, 100 nm. **a**–**d** reprinted from Stoffler et al. J Mol Biol 287:741–752 (1999) with permission from Elsevier. **e** and **f** reprinted from Stoffler et al. J Mol Biol 328:119–130 (2003) with permission from Elsevier

Such SFM experiments of the nuclear face of completely unfixed NEs revealed the repeated opening and closing of the nuclear baskets of the NPCs at their distal end in response to removing or adding (Fig. 4a,b) calcium. More specifically, the observed structural changes were such that 20 to 30 nm-diameter openings at the distal end of the baskets occurred upon addition of micromolar amounts of calcium without, however, affecting the overall height of the baskets (Stoffler et al. 1999b). This reversible structural change of the nuclear baskets may be interpreted in terms of their distal ring acting as an 'iris-like' diaphragm, as was previously suggested (Pante and Aebi 1996a), which is closed in the absence of calcium (Fig. 4a) and opens upon the addition of calcium (Fig. 4b). This observation also highlights the model by Akey (1990) who described the conformational changes of the NPC transporter mechanism as consisting of an iris-like mechanism based on analysis of cryoelectron microscopy images.

As the SFM is a surface sensor, it allows recording the surface topography of a given sample rather than its internal structure. As the structural change monitored on the nuclear surface of the NPC in response to adding or removing calcium clearly occurs at its highest elevation above the nuclear membrane surface (see the radial height profiles in Fig. 4a,b), it has to involve the distal ring of the nuclear basket. Obviously, it cannot be ruled out that changes may also occur in the interior of the NPC; however, these changes cannot be monitored by SFM as they are inaccessible to the scanning tip.

To explore the possibility of internal conformational changes of the NPC in response to calcium, EFTEM images of completely unfixed/unstained spread NEs embedded in a thick layer (i.e., 400 nm) of amorphous ice were recorded. As documented in Fig. 4c,d, single-particle averages of 100 NPC projection images of each sample incubated with and without calcium before freezing revealed significant structural rearrangements within the entire NPC. Whereas a detailed understanding of the structural changes occurring in response to adding or removing micromolar amounts of calcium to the NPC has to await tomographic reconstructions, the EFTEM-based projection data displayed in Fig. 4 are clearly consistent with our interpretation of the corresponding SFM data, for example, involving the nuclear basket's distal ring opening and closing like an iris diaphragm.

The central plug—a controversial element of the nuclear pore complex

As outlined above, 3-D reconstructions of the above-mentioned *dform Xenopus* NPCs and of yeast NPCs yielded a massive, elongated 'transporter' particle residing in the central pore (Akey and Radermacher 1993; Yang et al. 1998). Based on TEM and FEISEM data of *Chironomus* NPCs, this transporter appeared to be composed of two coaxial tubes and two globular assemblies that are symmetrically positioned about the NPC's midplane. This transporter was thought to undergo distinct and reversible conformational changes (Kiseleva et al. 1998). In contrast, depending on isolation, sample handling, and specimen preparation, earlier EM data have documented the abundance and the overall size and shape of the central plug to being highly variable (Pante and Aebi 1996a). The latest tomographic 3-D reconstruction of native vertebrate NPCs embedded in thick amorphous ice yielded a rather tenuous solid particle residing in the central pore whose mass amounted to about 40% of that of the distal ring (see Fig. 3b). Subaverages computed from this data set revealed this particle to be highly variable in terms of its overall size and shape, indicating that it might predominantly represent cargo caught in transit rather than a bona fide NPC component, i.e., a transporter (see below). Recently, similar observations were made in transport-active, intact nuclei of *D. discoideum* by cryoelectron tomography, which further supports the notion that the central plug essentially represents cargo caught in transit (Beck et al. 2004).

Time-lapse SFM experiments suggest that there exists a direct correlation between the transport state of the NPCs and the abundance of material obstructing the central pore (Stoffler et al. 2003). Accordingly, nucleocytoplasmic transport can be arrested at 4°C (Pante and Aebi 1996b; Pante et al. 1997). Native NEs as described above were first imaged in an optimal transport state (i.e., at 25°C). Here, the central pores appeared mostly unplugged (Fig. 4e). In a transport-inhibited state (i.e., at 4°C), the central pores appeared obstructed by cargo arrested in transit (Fig. 4f). Under these low force scanning conditions, it is highly unlikely that, for example, the central mass could be displaced from the central pore by the scanning tip without visibly compromising the cytoplasmic ring moiety. As to the nature of the central plug depicted in 2-D projection images of the NPC (see Fig. 2b), it represents for the larger part the distal ring of the nuclear basket located above the central pore, and as a more variable contribution, it is cargo in transit through the central pore.

Nucleocytoplasmic transport across the nuclear pore complex: the key ingredients

Deeper insight into the translocation mechanism can be obtained by correlating structural studies with biochemical findings. Nucleocytoplasmic transport proceeds when receptors of the karyopherin family (e.g., importins) recognize specific sequences found on cargo molecules in the form of nuclear import signals (NLSs) or nuclear export signals (Fried and Kutay 2003; Mosammaparast and Pemberton 2004). Transport receptors, in turn, are able to chaperone the cargo–receptor complex through the NPC via interactions between hydrophobic residues exposed on the receptor surface and the phenylalanine ring of FG-rich nucleoporins (Bayliss et al. 2000, 2002; Fribourg et al. 2001; Grant et al. 2003). In the case of nuclear import, the subsequent binding of RanGTP to the import receptor (i.e., importin-β) then induces the dissociation of the import

receptor from the FG-nucleoporin and releases the respective NLS-cargo into the nucleus (Rexach and Blobel 1995).

Importantly, FG-nucleoporins are mostly large proteins, which exhibit low overall hydrophobicity with their FG-repeat domains being natively unfolded (Denning et al. 2002, 2003). Natively unfolded proteins are known to exhibit multiple binding domains and are thus capable of simultaneous interactions with a large variety of binding partners (Dunker et al. 2001). Such characteristic behavior is manifested in FG-nucleoporins, which may be vital to achieve the fast transport rates observed with nucleocytoplasmic transport (Ribbeck and Gorlich 2001). More specifically, this includes: (1) exhibiting a high degree of flexibility and mobility (Fahrenkrog et al. 2002; Paulillo et al. 2005), (2) being able to interact simultaneously with several binding partners (Allen et al. 2001), and (3) promoting fast molecular association and dissociation rates (Gilchrist et al. 2002). In addition, immuno-EM studies of yeast NPCs reveal that FG-nucleoporins are predominantly located at the two facial peripheries of the NPC (Rout et al. 2000). Specifically, the majority of FG-nucleoporins are symmetric (i.e., located on the cytoplasmic and nuclear face of a NPC), while smaller numbers are found to be asymmetric (i.e., located exclusively on one side) (Rout et al. 2000). These natively unfolded FG-nucleoporins are postulated to pose a substantial barrier to nonreceptor cargo while providing for a high FG-density interaction zone for receptor-mediated cargo (see discussion below).

Nup153 is a well-studied FG-nucleoporin, which is known to be critical for both nuclear import and nuclear export (Shah et al. 1998; Ullman et al. 1999; for review see Ball and Ullman 2005). Immuno-EM studies of the vertebrate Nup153 have clearly demonstrated a high degree of mobility and structural flexibility of its FG-repeat domain (Fahrenkrog et al. 2002). Nup153 is a constituent of the nuclear basket of the NPC (Pante et al. 1994), where its N-terminal domain is anchored to the nuclear ring (Walther et al. 2001; Fahrenkrog et al. 2002), while its central zinc-finger domain resides at the distal ring (Fahrenkrog et al. 2002). In contrast, the ~700-residue long C-terminal domain of Nup153 harbors ~40 FG-repeats and appears to be flexible within the NPC, as it can be detected at any place within the nuclear basket and may even reach through the central pore and appear at its cytoplasmic periphery (Fahrenkrog et al. 2002).

The FG-rich C-terminal domain of Nup153 exhibits a relatively high binding affinity for importin β (Ben-Efraim and Gerace 2001) and acts as a terminal docking site for nuclear import cargoes (Shah et al. 1998). It is hypothesized that the long, mobile FG-rich C-terminal domain of Nup153 that is tethered to the distal ring via Nup153's Zn-finger domain, is able to bind cargo located anywhere within its reach, even close to the cytoplasmic side of the central pore. Therefore, these highly mobile FG-repeat domains may increase the efficiency of cargo translocation through the NPC (Paulillo et al. 2005).

Perspective: how to 'get to the bottom' of the nuclear pore complex

In spite of the progress made in understanding NPC structure and its implications for nucleocytoplasmic transport, several aspects of how individual NPCs facilitate cargo translocation remain unresolved. Such uncertainties stem from the complex nature of NPCs and from limitations associated with the current experimental approaches used to probe the NPC mechanism at the nanomolecular level. One of the controversies surrounding the field involves the origin of the 'paradoxical' selective gating mechanism/permeability barrier, which remains largely unknown. Based on strong indications that the barrier is formed by the FG-repeat domains, several attempts have been made to model and make sense of the plausible translocation mechanisms (Rout et al. 2000; Ben-Efraim and Gerace 2001; Macara 2001; Ribbeck and Gorlich 2002). The Brownian affinity gate model (Rout et al. 2000, 2003) proposes that the entropic behavior of peripheral FG-repeat nucleoporins acts as a substantial barrier to inert cargo. A higher probability of translocation is anticipated for receptor-mediated cargo due to interactions between the FG-repeats and the transport receptor, which facilitates entry into the pore where translocation then proceeds by Brownian motion. The affinity gradient model (Ben-Efraim and Gerace 2001) suggests that transport complexes 'step' through NPCs lined by FG-nucleoporins exhibiting increasing binding affinities with the cargo complexes. The 'oily spaghetti' model (Macara 2001) postulates that the NPC is filled with noninteracting FG-nucleoporins pushed aside by cargo complexes but otherwise obstruct the passage of passive cargo. Lastly, the selective phase model (Ribbeck and Gorlich 2002) predicts that FG-nucleoporins located within the central pore attract each other through hydrophobic inter-FG-repeat interactions resulting in the formation of a hydrophobic gel or meshwork. The selective phase then acts as a sieve that hinders the passage of passive cargo, while at the same time promotes the translocation of cargo complexes, which are able to dissolve through it.

To add to the complexity, findings based on *Saccharomyces cerevisiae* mutants, with asymmetric FG-repeats either swapped or deleted, show that the asymmetry of FG-nucleoporins is dispensable for bulk transport to proceed (Zeitler and Weis 2004). On a similar note, protein import through NPCs remains unaffected after removal of the cytoplasmic filaments (Walther et al. 2002). It is even more puzzling that a reduction in permeability is not observed in FG-repeat reduced minimal yeast NPCs (Strawn et al. 2004). To recapitulate, such ambiguities fall beyond the overall structural aspects of an NPC and instead pertain to local molecular effects, which occur in the near-field of an NPC, such as:

1. What constitutes the underlying selective gating mechanism/permeability barrier in NPCs?
2. What is the dynamic nature of the FG-repeat domains?

3. How do FG-repeats interact with transport receptors so as to promote cargo translocation rather than hinder it?
4. Does transport occur in a bidirectional manner? If so, how does the bidirectional import and export of receptor-bound cargoes occur simultaneously through an NPC with respect to spatial limitations and confinement effects within the central pore?
5. How do these effects promote the observed fast overall transport rates?
6. How do environmental conditions and effects, such as macromolecular crowding (Zimmerman and Minton 1993), affect the behavior of FG-nucleoporins and nucleocytoplasmic transport?

It is clear that the elucidation of complex nanoscale effects, such as those described above, necessitate the need to probe and understand the behavior of individual components of the NPC. Besides the work of Rexach and coworkers (Denning et al. 2003), little effort has been made into studying the molecular aspects of individual FG-nucleoporins, which is surprising given the fundamental importance of such molecules. To illustrate this point, we have used SFM to image the C-terminal FG-repeat domain of Nup153 as shown in Fig. 5. Although in this case the protein is physically adsorbed to the surface of mica, it is rather straightforward to see that it is indeed lacking structure and resembles an unfolded chain. From this image, we find that the molecule is ~200 nm long and has a cross-sectional width of 0.4 nm. These values correlate closely to the expected theoretical estimates of its length and diameter (e.g., size of a single aa) and verify that it is natively unfolded.

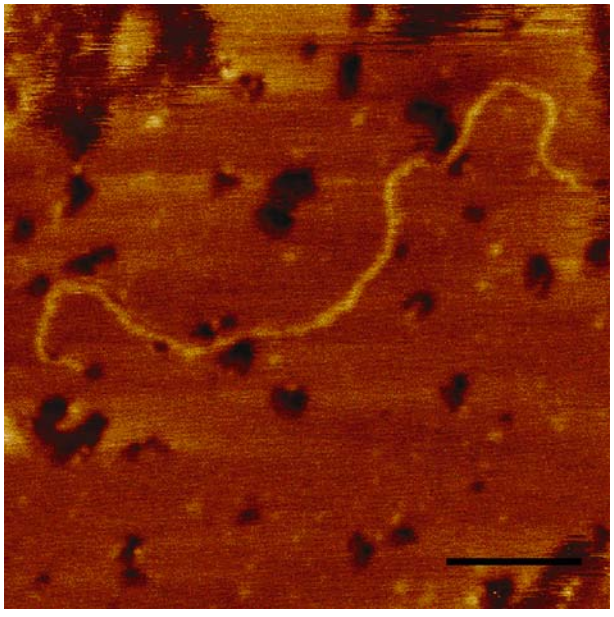

Fig. 5 Tapping mode SFM image (taken in air) of an individual molecule of the FG-rich C-terminal domain of human Nup153 adsorbed onto mica and dried. The molecule is ~180-nm long, has a cross-sectional diameter of 0.4 nm and strongly resembles an unfolded polypeptide chain. Scale Bar, 30 nm

Given the amount of conjecture of what may constitute the underlying mechanism of the selective gate-barrier, one needs to consider conducting experiments to explore the physical behavior of such FG-repeat domains at the relevant length and time scales. In our laboratory, we have designed an experimental platform to enable such experiments to be carried out. For example, SFM force measurements indicate that the collective behavior of clusters of the C-terminal FG-repeat domain of Nup153 surface-tethered to isolated Au nanodots (diameter ~100 nm) exert a long-ranged repulsive force characteristic of a brush-like molecular conformation (R.Y.H. Lim et al., submitted for publication). Such behavior was originally postulated by Rout et al. (2000) and is consistent with the fact that FG-domains are natively unfolded and flexible. Taking into consideration that the distribution of FG-nucleoporins lies predominantly on the periphery of either face of an NPC (Rout et al. 2000), our results indicate that the brush-like behavior of FG-repeat domains can manifest as a significant entropic barrier over an NPC, which exerts a long-ranged repulsive force that scales with the size of an approaching particle (i.e., small molecules such as ions and water diffuse more easily through). In this event, while oncoming passive cargo in the NPC near field will be repelled by this barrier, receptor-mediated NLS-cargo will instead end up being 'trapped' because of binding interactions, which occur between the transport receptor and various FG-sites. Our findings also indicate that a small number (~10) of FG-nucleoporins is enough to maintain the entropic barrier in native NPCs. It is worthwhile noting that this could explain why a reduction in NPC permeability was not detected in FG-repeat

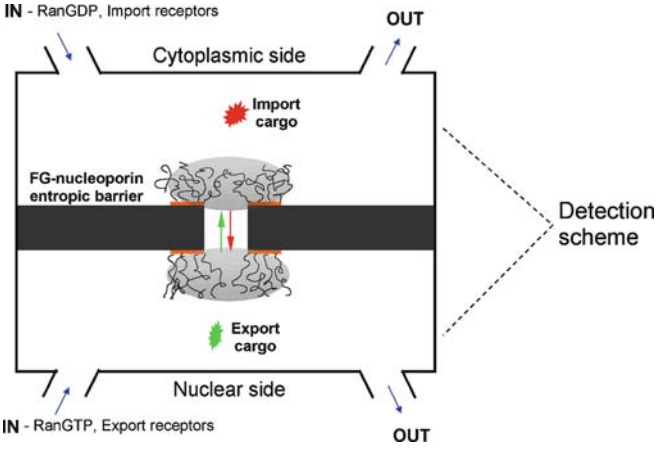

Fig. 6 Schematic illustration of a de novo designed 'minimalist' NPC. The design consists of identifying key components of the NPC (e.g., FG-nucleoporins, transport receptors, RanGTP/GDP) and integrating them into an artificial setup. Ideally, the core of such a setup would comprise of a membrane perforated with nanometer-sized holes. FG-nucleoporins would then be covalently tethered to the surface surrounding each hole. The rest of the setup consists of a two-chamber system, which separates either side of the porous membrane, mimicking the cytoplasmic side and nuclear side of a nucleus. Inlets and outlets would carry experimentally controlled amounts of transport receptors, cargo, and Ran to each respective side. Various detection schemes can then be adapted to monitor the transport of cargo through the de novo NPC

reduced minimal yeast NPCs (Strawn et al. 2004). Remarkably, the brush-like behavior of C-terminal Nup153 FG-repeat clusters can be induced to undergo a reversible collapse by the addition/removal of a less polar solvent (i.e., 1,2-hexanediol) to the buffer (R.Y.H. Lim et al., submitted for publication). Importantly, these results mirror the reversible collapse of the permeability barrier, as observed by Ribbeck and Gorlich (2002), and validates the hypothesis that FG-nucleoporins form the major constituents of such a barrier in native NPCs. With respect to inter-FG interactions, certainly more experimentation is required, but we postulate that they are most likely highly dynamic at much shorter time scales (as opposed to being a quasistatic meshwork; cf. Ribbeck and Gorlich 2002), which may serve to enhance the overall effectiveness of such a barrier.

We advise with caution that none of these findings are adequate to provide for a complete picture of how translocation proceeds for trapped receptor-mediated cargo. Although the directionality of transport would be driven predominantly by the RanGTP gradient across the two sides of the NPC to create a continuous bidirectional cascade of cargo (Izaurralde et al. 1997; Richards et al. 1997), we concur that after being captured, the process by which cargo complexes negotiate the high density FG-barrier and are funneled into the central pore through weak and transient, rather than strong interactions, is as yet unknown. Nevertheless, the application of single molecule optical approaches by Peters and coworkers to study the kinetics of molecular transport through NPCs may provide further insight into such effects (Keminer and Peters 1999; Radtke et al. 2001; Kiskin et al. 2003; Hoppener et al. 2005; Kubitscheck et al. 2005).

Besides experimental work, perhaps another meaningful approach to dissect such complex effects involves the use of computational techniques (Bickel and Bruinsma 2002; Kustanovich and Rabin 2004) and molecular dynamics (MD) simulations (Isgro and Schulten 2005). In the NPC field, a recent MD simulation by Isgro and Schulten (2005) was able to replicate the binding sites of FG-repeats to importin-β. The predictive capabilities of such work is convincingly shown by being able to predict an additional binding site that has only been recently discovered experimentally (Liu and Stewart 2005) after completion of the MD work. Besides further predicting additional binding sites on importin-β not yet observed experimentally, the MD simulation is able to show that without any importin-β present, short FG-repeat segments have a tendency to interact with each other within the time scale of the simulation, i.e., ~50 ns (Isgro and Schulten 2005).

This discussion underscores the following: (1) the key components guiding nucleocytoplasmic transport need to be individually understood, (2) the NPC is dynamic and requires experimental/computational procedures to study phenomenon at the relevant length/time scales, and (3) the need to move beyond classical biology and to adopt more interdisciplinary concepts and approaches. For example, identifying and integrating the key components (e.g., FG-nucleoporins, the Ran-GTP cycle, transport receptors, etc.) into an experimental platform with the purpose of functioning as a de novo designed 'minimalist' NPC (Fig. 6) may circumvent the difficulties associated with studying individual native NPCs. Ideally, it is plausible to mimic the nucleocytoplasmic transport phenomenon and allow for a wide range of experimental detection schemes. As we persevere to get to the bottom of the nuclear pore complex, perhaps such a 'minimalist' approach can bring new understanding to nucleocytoplasmic transport by correlating such experiments with biochemical findings.

Acknowledgements This work was supported by the M.E. Müller Foundation of Switzerland, the 'EU Network of Excellence 3D-EM' project no. LSHG-CT-2004-502828, and the Swiss National Science Foundation through the National Centre of Competence (NCCR) in Nanoscale Science (Nanobiology). The authors would like to thank Dr. Birthe Fahrenkrog for providing us with Fig. 2a, and Dr. Bohumil Maco for providing us with Fig. 2c,d.

References

Aebi U, Jarnik M, Reichelt, R, Engel A (1990) Structural analysis of the nuclear pore complex by conventional and scanning transmission electron microscopy (CTEM/STEM). EMSA Bull 20:69–76

Akey CW (1990) Visualization of transport-related configurations of the nuclear-pore transporter. Biophys J 58:341–355

Akey CW, Radermacher M (1993) Architecture of the Xenopus nuclear pore complex revealed by three-dimensional cryo-electron microscopy. J Cell Biol 122:1–19

Allen NPC, Huang L, Burlingame A, Rexach M (2001) Proteomic analysis of nucleoporin interacting proteins. J Biol Chem 276:29268–29274

Ball JR, Ullman KS (2005) Versatility at the nuclear pore complex: lessons learned from the nucleoporin Nup153. Chromosoma 114(5):319–330

Bayliss R, Littlewood T, Stewart M (2000) Structural basis for the interaction between FxFG nucleoporin repeats and importin-beta in nuclear trafficking. Cell 102:99–108

Bayliss R, Littlewood T, Strawn LA, Wente SR, Stewart M (2002) GLFG and FxFG nucleoporins bind to overlapping sites on importin-beta. J Biol Chem 277:50597–50606

Beck M, Forster F, Ecke M, Plitzko JM, Melchior F, Gerisch G, Baumeister W, Medalia O (2004) Nuclear pore complex structure and dynamics revealed by cryoelectron tomography. Science 306:1387–1390

Ben-Efraim I, Gerace L (2001) Gradient of increasing affinity of importin beta for nucleoporins along the pathway of nuclear import. J Cell Biol 152:411–417

Bickel T, Bruinsma R (2002) The nuclear pore complex mystery and anomalous diffusion in reversible gels. Biophys J 83:3079–3087

Braunstein D, Spudich A (1994) Structure and activation dynamics of RBL-2H3 cells observed with scanning force microscopy. Biophys J 66:1717–1725

Bustamante JO, Michelette ER, Geibel JP, Dean DA, Hanover JA, McDonnell TJ (2000) Calcium, ATP and nuclear pore channel gating. Pflugers Arch 439:433–444

Cohen M, Tzur YB, Neufeld E, Feinstein N, Delannoy MR, Wilson KL, Gruenbaum Y (2002) Transmission electron microscope studies of the nuclear envelope in Caenorhabditis elegans embryos. J Struct Biol 140:232–240

Cordes VC, Reidenbach S, Rackwitz HR, Franke WW (1997) Identification of protein p270/Tpr as a constitutive component of the nuclear pore complex-attached intranuclear filaments. J Cell Biol 136:515–529

Denning DP, Uversky V, Patel SS, Fink AL, Rexach M (2002) The Saccharomyces cerevisiae nucleoporin Nup2p is a natively unfolded protein. J Biol Chem 277:33447–33455

Denning DP, Patel SS, Uversky V, Fink AL, Rexach M (2003) Disorder in the nuclear pore complex: The FG repeat regions of nucleoporins are natively unfolded. Proc Natl Acad Sci USA 100:2450–2455

Dunker AK, Lawson JD, Brown CJ, Williams RM, Romero P, Oh JS, Oldfield CJ, Campen AM, Ratliff CR, Hipps KW, Ausio J, Nissen MS, Reeves R, Kang CH, Kissinger CR, Bailey RW, Griswold MD, Chiu M, Garner EC, Obradovic Z (2001) Intrinsically disordered protein. J Mol Graph Model 19:26–59

Fahrenkrog B, Aebi U (2002) The vertebrate nuclear pore complex: from structure to function. Results Probl Cell Differ 35:25–48

Fahrenkrog B, Aebi U (2003) The nuclear pore complex: nucleocytoplasmic transport and beyond. Nat Rev Mol Cell Biol 4:757–766

Fahrenkrog B, Hurt EC, Aebi U, Pante N (1998) Molecular architecture of the yeast nuclear pore complex: localization of Nsp1p subcomplexes. J Cell Biol 143:577–588

Fahrenkrog B, Maco B, Fager AM, Koser J, Sauder U, Ullman KS, Aebi U (2002) Domain-specific antibodies reveal multiple-site topology of Nup153 within the nuclear pore complex. J Struct Biol 140:254–267

Folprecht G, Schneider S, Oberleithner H (1996) Aldosterone activates the nuclear pore transporter in cultured kidney cells imaged with atomic force microscopy. Pflugers Arch 432:831–838

Fribourg S, Braun IC, Izaurralde E, Conti E (2001) Structural basis for the recognition of a nucleoporin FG repeat by the NTF2-like domain of the TAP/p15 mRNA nuclear export factor. Mol Cell 8:645–656

Fried H, Kutay U (2003) Nucleocytoplasmic transport: taking an inventory. Cell Mol Life Sci 60:1659–1688

Gilchrist D, Mykytka B, Rexach M (2002) Accelerating the rate of disassembly of karyopherin center dot cargo complexes. J Biol Chem 277:18161–18172

Goldberg MW, Wiese C, Allen TD, Wilson KL (1997) Dimples, pores, star-rings, and thin rings on growing nuclear envelopes: evidence for structural intermediates in nuclear pore complex assembly. J Cell Sci 110(4):409–420

Goldie KN, Pante N, Engel A, Aebi U (1994) Exploring native nuclear pore complex structure and conformation by scanning force microscopy in physiological buffers. J Vac Sci Technol B 1482–1485

Grant RP, Neuhaus D, Stewart M (2003) Structural basis for the interaction between the Tap/NXF1 UBA domain and FG nucleoporins at 1A resolution. J Mol Biol 326:849–858

Hinshaw JE, Carragher BO, Milligan RA (1992) Architecture and design of the nuclear pore complex. Cell 69:1133–1141

Hoppener C, Siebrasse JP, Peters R, Kubitscheck U, Naber A (2005) High-resolution near-field optical imaging of single nuclear pore complexes under physiological conditions. Biophys J 88:3681–3688

Isgro TA, Schulten K (2005) Binding dynamics of isolated nucleoporin repeat regions to importin-ß. Structure in press

Izaurralde E, Kutay U, vonKobbe C, Mattaj IW, Gorlich D (1997) The asymmetric distribution of the constituents of the Ran system is essential for transport into and out of the nucleus. EMBO J 16:6535–6547

Jaggi RD, Franco-Obregon A, Ensslin K (2003a) Quantitative topographical analysis of nuclear pore complex function using scanning force microscopy. Biophys J 85:4093–4098

Jaggi RD, Franco-Obregon A, Muhlhausser P, Thomas F, Kutay U, Ensslin K (2003b) Modulation of nuclear pore topology by transport modifiers. Biophys J 84:665–670

Jarnik M, Aebi U (1991) Toward a more complete 3-D structure of the nuclear pore complex. J Struct Biol 107:291–308

Keminer O, Peters R (1999) Permeability of single nuclear pores. Biophys J 77:217–228

Kiseleva E, Goldberg MW, Allen TD, Akey CW (1998) Active nuclear pore complexes in Chironomus: visualization of transporter configurations related to mRNP export J Cell Sci 111(2):223–236

Kiskin NI, Siebrasse JP, Peters R (2003) Optical microwell assay of membrane transport kinetics. Biophys J 85:2311–2322

Kubitscheck U, Grunwald D, Hoekstra A, Rohleder D, Kues T, Siebrasse JP, Peters R (2005) Nuclear transport of single molecules: dwell times at the nuclear pore complex. J Cell Biol 168:233–243

Kustanovich T, Rabin Y (2004) Metastable network model of protein transport through nuclear pores. Biophys J 86:2008–2016

Liu SM, Stewart M (2005) Structural basis for the high-affinity binding of nucleoporin Nup1p to the Saccharomyces cerevisiae importin-beta homologue, Kap95p. J Mol Biol 349:515–525

Macara IG (2001) Transport into and out of the nucleus. Microbiol Mol Biol Rev 65:570

Mosammaparast N, Pemberton LF (2004) Karyopherins: from nuclear-transport mediators to nuclear-function regulators. Trends Cell Biol 14:547–556

Oberleithner H, Brinckmann E, Schwab A, Krohne G (1994) Imaging nuclear pores of aldosterone-sensitive kidney cells by atomic force microscopy. Proc Natl Acad Sci USA 91:9784–9788

Oberleithner H, Schneider S, Bustamante JO (1996) Atomic force microscopy visualizes ATP-dependent dissociation of multimeric TATA-binding protein before translocation into the cell nucleus. Pflugers Arch 432:839–844

Pante N, Aebi U (1993) The nuclear pore complex. J Cell Biol 122:977–984

Pante N, Aebi U (1996a) Molecular dissection of the nuclear pore complex. Crit Rev Biochem Mol Biol 31:153–199

Pante N, Aebi U (1996b) Sequential binding of import ligands to distinct nucleopore regions during their nuclear import. Science 273:1729–1732

Pante N, Bastos R, McMorrow I, Burke B, Aebi U (1994) Interactions and three-dimensional localization of a group of nuclear pore complex proteins. J Cell Biol 126:603–617

Pante N, Jarmolowski A, Izaurralde E, Sauder U, Baschong W, Mattaj IW (1997) Visualizing nuclear export of different classes of RNA by electron microscopy. RNA 3:498–513

Paulillo SM, Phillips EM, Koser J, Sauder U, Ullman KS, Powers MA, Fahrenkrog B (2005) Nucleoporin domain topology is linked to the transport status of the nuclear pore complex. J Mol Biol 351:784–798

Perez-Terzic C, Pyle J, Jaconi M, Stehno-Bittel L, Clapham DE (1996) Conformational states of the nuclear pore complex induced by depletion of nuclear $Ca2^{+}$ stores. Science 273:1875–1877

Radtke T, Schmalz D, Coutavas E, Soliman TM, Peters R (2001) Kinetics of protein import into isolated Xenopus oocyte nuclei. Proc Natl Acad Sci USA 98:2407–2412

Rakowska A, Danker T, Schneider SW, Oberleithner H (1998) ATP-induced shape change of nuclear pores visualized with the atomic force microscope. J Membr Biol 163:129–136

Reichelt R, Holzenburg A, Buhle EL Jr, Jarnik M, Engel A, Aebi U (1990) Correlation between structure and mass distribution of the nuclear pore complex and of distinct pore complex components. J Cell Biol 110:883–894

Rexach M, Blobel G (1995) Protein import into nuclei—association and dissociation reactions involving transport substrate, transport factors, and nucleoporins. Cell 83:683–692

Ribbeck K, Gorlich D (2001) Kinetic analysis of translocation through nuclear pore complexes. EMBO J 20:1320–1330

Ribbeck K, Gorlich D (2002) The permeability barrier of nuclear pore complexes appears to operate via hydrophobic exclusion. EMBO J 21:2664–2671

Richards SA, Carey KL, Macara IG (1997) Requirement of guanosine triphosphate-bound Ran for signal-mediated nuclear protein export. Science 276:1842–1844

Ris H (1989) Three-dimensional structure of the nuclear pore complex. J Cell Biol 109:134a

Ris H (1997) High-resolution field-emission scanning electron microscopy of nuclear pore complex. Scanning 19:368–375

Ris H, Malecki M (1993) High-resolution field-emission scanning electron-microscope imaging of internal cell structures after epon extraction from sections—a new approach to correlative ultrastructural and immunocytochemical studies. J Struct Biol 111:148–157

Rout MP, Blobel G (1993) Isolation of the yeast nuclear pore complex. J Cell Biol 123:771–783

Rout MP, Aitchison JD, Suprapto A, Hjertaas K, Zhao Y, Chait BT (2000) The yeast nuclear pore complex: composition, architecture, and transport mechanism. J Cell Biol 148:635–651

Rout MP, Aitchison JD, Magnasco MO, Chait BT (2003) Virtual gating and nuclear transport: the hole picture. Trends Cell Biol 13:622–628

Sanner MF, Stolz M, Burkhard P, Kong XP, Min G, Sun TT, Driamov S, Aebi U, Stoffler D (2005) Visualizing nature at work from the nano to the macro scale. Nanobiotechnology 1:7–21

Shah S, Tugendreich S, Forbes D (1998) Major binding sites for the nuclear import receptor are the internal nucleoporin Nup153 and the adjacent nuclear filament protein Tpr. J Cell Biol 141:31–49

Stoffler D, Fahrenkrog B, Aebi U (1999a) The nuclear pore complex: from molecular architecture to functional dynamics. Curr Opin Cell Biol 11:391–401

Stoffler D, Goldie KN, Feja B, Aebi U (1999b) Calcium-mediated structural changes of native nuclear pore complexes monitored by time-lapse atomic force microscopy. J Mol Biol 287:741–752

Stoffler D, Feja B, Fahrenkrog B, Walz J, Typke D, Aebi U (2003) Cryo-electron tomography provides novel insights into nuclear pore architecture: implications for nucleocytoplasmic transport. J Mol Biol 328:119–130

Stolz M, Stoffler D, Aebi U, Goldsbury C (2000) Monitoring biomolecular interactions by time-lapse atomic force microscopy. J Struct Biol 131:171–180

Strawn LA, Shen T, Shulga N, Goldfarb DS, Wente SR (2004) Minimal nuclear pore complexes define FG repeat domains essential for transport. Nat Cell Biol 6:197–206

Ullman KS, Shah S, Powers MA, Forbes DJ (1999) The nucleoporin nup153 plays a critical role in multiple types of nuclear export. Mol Biol Cell 10:649–664

Walther TC, Fornerod M, Pickersgill H, Goldberg M, Allen TD, Mattaj IW (2001) The nucleoporin Nup153 is required for nuclear pore basket formation, nuclear pore complex anchoring and import of a subset of nuclear proteins. EMBO J 20:5703–5714

Walther TC, Pickersgill HS, Cordes VC, Goldberg MW, Allen TD, Mattaj IW, Fornerod M (2002) The cytoplasmic filaments of the nuclear pore complex are dispensable for selective nuclear protein import. J Cell Biol 158:63–77

Wang HW, Clapham DE (1999) Conformational changes of the in situ nuclear pore complex. Biophys J 77:241–247

Yang Q, Rout MP, Akey CW (1998) Three-dimensional architecture of the isolated yeast nuclear pore complex: functional and evolutionary implications. Mol Cell 1:223–234

Zeitler B, Weis K (2004) The FG-repeat asymmetry of the nuclear pore complex is dispensable for bulk nucleocytoplasmic transport in vivo. J Cell Biol 167:583–590

Zimmerman SB, Minton AP (1993) Macromolecular crowding—biochemical, biophysical, and physiological consequences. Annu Rev Biophys Biomol Struct 22:27–65